THE PENNSYLVANIA STATE UNIVERSITY
SCHREYER HONORS COLLEGE

DEPARTMENT OF METEOROLOGY

INVESTIGATION OF A POSSIBLE SOLUTION TO THE FAINT YOUNG SUN PARADOX: ELEMENTAL SULFUR AEROSOLS

MEGAN LEIGH SMITH

Spring 2010

A thesis
submitted in partial fulfillment
of the requirements
for a baccalaureate degree
in Meteorology
with honors in Meteorology

Reviewed and approved* by the following:

James F. Kasting
Distinguished Professor of Geosciences
Thesis Supervisor

Paul Markowski
Associate Professor of Meteorology
Honors Adviser

Hampton N. Shirer
Associate Professor of Meteorlogy
Faculty Reader

* Signatures are on file in the Schreyer Honors College

TABLE OF CONTENTS

ABSTRACT

In 1972, astronomers Carl Sagan and George Mullen presented the *faint young Sun paradox,* a discrepancy between the predicted subfreezing global surface temperature on the early Earth and geologic evidence of a warm planet. Standard models of solar evolution calculate that the Earth's surface temperature would have been below freezing until two billion years ago. Geologic evidence indicates that surface liquid water existed long before that time, however. Past research on solutions to this problem has yielded inconclusive results. Atmospheric particles (aerosols) absorb radiation, and may therefore be a possible solution to the problem. Here, two separate investigations of the representation of particles in one-dimensional models are made. First, treatment of particles in a photochemical model is validated, using Saturn's largest moon, Titan. The results compare well with observations of Titan's albedo spectrum. Second, an attempt to solve the *faint young Sun paradox* with elemental sulfur particles is made. The optical properties for these particles are inserted into a one-dimensional photochemical model and a one-dimensional radiative-convective climate model, both configured for the Late Archean/Paleoproterozoic era on Earth (2.2 to 2.8 billion years ago). Inclusion of the sulfur particles lowers the surface temperature by 3 K. Despite the negative outcome, future investigation may yield more encouraging results. Other sulfur allotropes, such as S_3 and S_4, may increase surface temperatures.

LIST OF FIGURES

ACKNOWLEDGMENTS

Support for this research comes from the Schreyer Honors College Summer 2009 Research Scholarship. The author would like to thank Dr. James Kasting for guidance and mentorship throughout this research project.

Chapter 1: Introduction to the Faint Young Sun Paradox and Related Research

According to standard models of solar evolution, the Sun's luminosity has increased linearly since it moved onto the main sequence 4.6 billion years ago. At the beginning of Solar System history, the Sun was only 70% as bright as it is today (Gough, 1981). Assuming that the composition of Earth's atmosphere has not changed over the course of geologic time, the global surface temperature would have been below freezing until around two billion years ago. Geologic and paleontological evidence suggests, however, that liquid water was present on Earth's surface at least 3.5 billion years ago. In 1972, astronomers Carl Sagan and George Mullen presented this conundrum, which later became known as the *faint young Sun paradox*. Since this paradox was recognized, research on possible solutions has been accumulating. The preferred solution to the paradox is greenhouse warming, but constraints from the geologic record and photochemical behavior of gases place an upper limit on the mixing ratios of certain constituents in the ancient atmosphere.

Previous climate modeling of the early Earth, in particular the Late Archean/ Paleoproterzoic (2.2 to 2.8 billion years ago), has focused on solving the faint young Sun paradox with greenhouse gases such as NH_3, CO_2, CH_4, and C_2H_6. Particulate matter in the atmosphere, known as aerosols, also contributes to the radiative forcing felt at the surface. Previous research suggests that elemental sulfur aerosols (S_8) absorb ultraviolet radiation (Kasting et al., 1989), and therefore these particles may increase the global surface temperature. Here, I input elemental sulfur particles (S_8) into one-dimensional photochemical and climate models in order to estimate their effects on the surface temperature.

I began by investigating the validity of the photochemical model by replicating measurements of Saturn's moon Titan. Titan is interesting to planetary scientists because of its dense atmosphere composed of mostly N_2 and CH_4, making it a possible analog to the early Earth. I was able to reproduce measurements of Titan's geometric albedo spectrum, meaning that the model correctly captured ultraviolet absorption by the hydrocarbon aerosols. Having confirmed the treatment of particles within the model, I next could include sulfur aerosols in the photochemical model.

Today our Sun has luminosity L of $3.84*10^{26}$ W. The flux received at a distance d,

$$f = \frac{L}{4\pi d^2} \qquad (1)$$

in combination with the greenhouse effect, keeps Earth's surface warm enough for liquid water, an essential component of life as we know it. If both L and d stay constant over time, then the solar flux at Earth is a constant. The Sun-Earth distance d is assumed to be constant since early in the geologic past. Current models show that planets settle into their orbits relatively quickly, within 200 million years (Raymond et al., 2006). The solar luminosity, however, increases over time owing to the nuclear fusion processes that occur within the core of the Sun (Hoyle et al., 1958; Haselgrove and Hoyle, 1959; Gough, 1981).

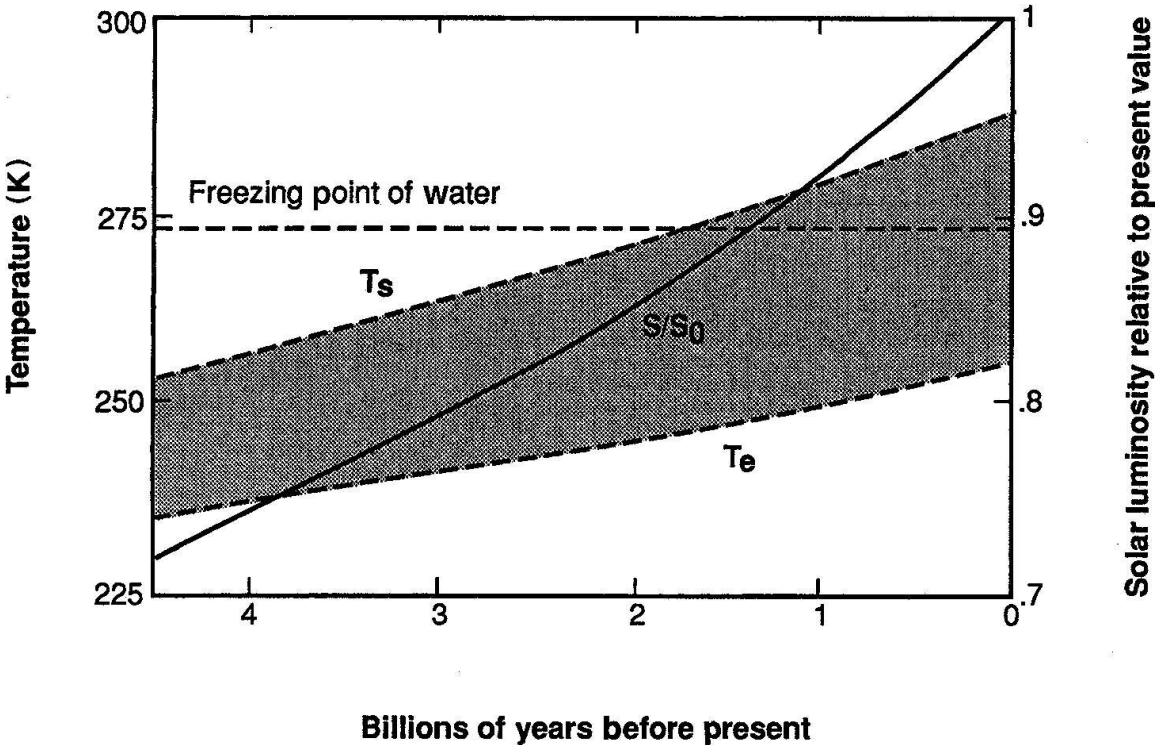

Fig. 1: The solid curve is the changing solar luminosity over time, as calculated by Gough (1981). The lower dashed curve is the effective temperature, T_e, calculated with a radiative-convective climate model. The upper dashed curve is the surface temperature, T_s, calculated in an atmosphere with 300 ppmv CO_2 and a fixed tropospheric relative humidity profile (Figure from Kasting et al.,1988).

As the Sun evolves, hydrogen is converted to helium. The core of the Sun consequently contracts and the central pressure rises (Gough, 1981). As the core contracts, the potential energy decreases and the kinetic energy increases. The temperature of the Sun thus increases and luminosity increases, as shown in Fig. 1. Gough (1981) presented (2) to describe the luminosity over time:

$$L(t) = [1+\frac{2}{5}(1-\frac{t}{t_*})]^{-1} L_* \qquad (2)$$

Here, t is time, t_* is the current time, and L_* is the current solar luminosity. At $t = 0$, 4.6 billion years ago, $L = 0.7L_*$.

Using an earlier estimate for the solar luminosity increase, Sagan and Mullen (1972) calculated Earth's effective temperature as a function of time, assuming that Earth's atmospheric composition had not evolved. The authors iteratively solved (3) for the global surface temperature T_s.

$$\frac{1}{4}S(1-A) = \sum_i e\ B_{\lambda i}(T_s)\Delta\lambda_i + \sum_j B_{\lambda j}(2^{-1/4}T_e)\Delta\lambda_j \qquad (3)$$

in which S is the solar constant, A is the Russell-Bond spherical albedo of the Earth, B_λ is the Planck specific intensity, e is the atmospheric emissivity, $\Delta\lambda$ is the wavelength interval, and T_e is the effective equilibrium temperature of the Earth. The term $2^{-1/4}T_e$ is the *skin temperature* of the Earth, an approximately isothermal outer boundary of the atmosphere that is in radiative equilibrium. When the model was run backward in time, the results indicated that the global surface temperature of the Earth would have been below freezing until two billion years ago (2 Ga). Later results from one-dimensional climate models corroborated this result (Kasting et al., 1988). Prior to around two billion years ago, it would appear to be physically impossible for surface liquid water to have existed. But, there is strong evidence suggesting that liquid water did exist on Earth's surface, long before 2 Ga. Pillow lavas, mud cracks, and ripple marks in the Swaziland group, a large suite of rocks over 3.2 billion years old, indicate the presence of water flow (Sagan and Mullen, 1972). Additionally, the oldest known stromatolites, microbial sedimentary structures that form in tidal pools date back to 3.5 Ga, providing strong evidence for surface liquid water at that time. So, a discrepancy emerges between model results and geologic evidence.

Evidence of past liquid water flow is not only present on Earth, but also on Mars. Images first taken by NASA's Mariner and Viking missions show fluvial features meandering their way across Mars' surface (Kasting et al., 1989). The existence of liquid water on early Mars is even more of a puzzle to scientists because the semi-major axis of Mars' orbit is 1.52 AU, so by (1) the solar flux at Mars's orbit is even smaller than the flux at Earth's orbit. Additionally, Mars' present atmosphere is tenuous because the surface pressure is 0.006 bars, and so greenhouse warming by CO_2 is minimal, around 6 K. In order to mitigate the cooling effects of the faint young Sun, scientists have been investigating both internal and external forcings that may have kept the surfaces of early Earth and early Mars wet.

In the calculations made by both Sagan and Mullen (1972) and Kasting et al. (1988), the atmospheres of both planets were assumed not to have changed over the course of geologic time. Atmospheres do evolve over time, however. For example, oxygen did not become a major constituent in Earth's atmosphere until around 2.4 billion years ago. Banded-iron formations, red beds, uranium ores, and paleosols all indicate a more reduced atmospheric state prior to this time (Holland, 1994). In a more reduced atmosphere, methane could have been more abundant than it is today. Calculations by Haqq-Misra et al. (2008) assume a methane volume mixing ratio of 1000 ppm. This value can be compared to a modern value of 1751 ppb (Dlugokencky et al., 2003). Also, paleosols, ancient soils, indicate that pCO_2 in the early Earth atmosphere may have been as high as 100 times the present atmospheric level (Haqq-Misra et al., 2008). As time progressed, changing sources and sinks of varying gases, escape of gases to space, and the role of feedback mechanisms between the atmosphere, surface, and biosphere all cause the atmosphere to change.

As mentioned above, atmospheric CO_2 and CH_4 could have been much more abundant in the geologic past. Both carbon dioxide and methane are greenhouse gases. Greenhouse gases absorb and re-emit infrared radiation that is emitted from the surface of the Earth, but they are relatively transparent to incoming solar radiation. Over the past few decades, scientists have become increasingly aware that anthropogenic emissions are increasing the mixing ratios of greenhouse gases in our atmosphere, and the planet is

warming. Greenhouse gases also can affect planetary energy balances over the course of geologic timescales. Venus, for example, has an atmosphere that is composed of a staggering 90 bars of CO_2. Venus has been in a runaway greenhouse state for a long time, because CO_2 is not able to be recycled within the mantle of the planet owing to the absence of liquid water and plate tectonics. Sagan and Mullen (1972) were the first authors to hypothesize that increased concentrations of greenhouse gases could have kept the early Earth warm and counteracted the faint young Sun. They thought that the ideal greenhouse gas for warming the early Earth would have been NH_3. Ammonia is a reduced gas, and could have been abundant in the atmosphere prior to the Great Oxidation Event of 2.4 billion years ago. The authors calculate that sub-equilibrium levels of NH_3 could have kept the surface temperature above freezing for all of Earth's history. But, others quickly pointed out that NH_3 rapidly photolyzes to N_2 and H_2, and so it would disappear quickly (Kasting, 1988). It is possible, however, that a higher layer of organic haze could have shielded ammonia from photolysis (Kasting, 1997).

Carbon dioxide is much more stable in the atmosphere than ammonia. It is also an efficient greenhouse gas. Understanding of the carbon-silicate cycle allows scientists to quantify the response of the climate system to changing CO_2 concentrations over long periods of time. The carbonate-silicate cycle is a negative feedback loop that regulates the amount of atmospheric CO_2 over geologic time. The cycle operates over a time scale of 500,000 years (Kasting et al., 1989). One possible pathway for the feedback loop is thus: increased levels of atmospheric CO_2 warm the surface, which in turn increases removal of atmospheric CO_2 by weathering, and as a result the atmosphere cools. The carbonate-silicate cycle feedback ensures that the mean surface temperature must have been above freezing, so that liquid water could have existed. It is possible, but controversial that the mean surface temperature was greater than this value (Kasting et al., 2006).

Because the carbon-silicate cycle is a negative feedback loop, elevated levels of carbon dioxide would not have pushed the Earth into a runaway greenhouse like that observed on Venus. The problem with a CO_2 solution to the faint young Sun paradox is that evidence for elevated levels of CO_2 is lacking. If carbon dioxide amounts were high -- around 300 times the current value -- then paleosols from 2.5 to 2.8 Ga would reveal CO_2 reacting with iron to form siderite, but they do not (Rye et al., 1995; Lunine, 2005). According to Haqq-Misra et al. (2008), the paleosol limits should not be rigid because of the inherent uncertainty of the data, however. Rye et al. (1995) place the upper limit of pCO_2 at 0.03 bars, which we use in our calculations. More recent estimates, however, place the upper limit of pCO_2 at $1*10^{-3}$ bars (Rosing et al., 2010).

Another constituent that likely was present in the early atmosphere is methane, which was produced mostly biologically by methanogens. Evidence for biogenically-produced methane in the atmosphere of the early Earth is found in fluid-inclusions in 3.5-billion- year old rocks in Pilbara, Australia (Ueno et al., 2006). A methane concentration of 100 ppmv would allow the atmospheric CO_2 concentration to decrease by a factor of 10 and still produce equivalent surface warming (Lunine, 2005). Methane therefore reduces the significance of CO_2, and so climate modelers are better able to conform to the CO_2 paleosol limits. In a more reduced atmosphere, the residence time of methane increases to around 10,000 years. Methane-producing microbes, methanogens, would accelerate the greenhouse effect owing to a direct correlation between atmospheric

warming and the methanogenesis rate (Haqq-Misra et al., 2008). In this case, a runaway greenhouse would be averted by the buildup of an optically thick haze formed by methane polymerization (Kasting, 2004). A thick haze would absorb solar radiation high in the stratosphere and re-emit it to space and induce an *antigreenhouse effect* similar to that seen on Saturn's moon, Titan. The *antigreenhouse effect* occurs when a layer of haze is optically thin in the infrared and optically thick in the visible. Assuming that such a layer is isothermal and has an emissivity less than unity, it then follows that the layer emits half of the incident solar radiation back to space and half of it toward the surface. The net effect is surface cooling; specifically, the surface temperature is reduced from the effective temperature by the factor $(1/2)^{1/4}$ (McKay et al., 1991) where the effective temperature is defined by the global energy balance equation

$$\frac{S}{4}(1-A) = \sigma T_e^{\,4} \qquad (4)$$

where S is the solar constant [Wm^{-2}], A is the bond albedo, σ is the Stefan-Boltzmann constant, and T_e is the effective temperature.

In addition to ammonia, carbon dioxide, and methane, there are other atmospheric constituents that can warm planetary surfaces. Ethane, C_2H_6, for example, in conjunction with carbon dioxide and methane, could have raised surface temperatures in the Late Archean/Paleoproterozoic (2.2 to 2.8 billion years ago) by up to 20 K (Haqq-Misra et al., 2008). Ethane is only largely present in a hydrocarbon-rich atmosphere, however. In such atmospheres, haze readily forms and the anti-greenhouse effect becomes substantial. As a result, Haqq-Misra et al. (2008) conclude that ethane would only have warmed the surface by a few degrees. Researchers continue to run into roadblocks when trying to counteract the faint young Sun with greenhouse gases.

Alternative Theories to the Faint Young Sun Paradox

It should be noted that there are other alternatives to solving the faint young Sun paradox, but most of them have critical faults. Several workers, for example, claim that if the fractional cloud-cover on the early Earth were lower than modern-day cloud cover, then a decreased planetary albedo would have increased the global surface temperature. This feedback would work if the early Earth were substantially cooler than today because of the exponential dependence of saturation vapor pressure on temperature (Rosing et al., 2010; Rondanelli and Lindzen, 2010). There is much debate on the temperature of the early Earth relative to today. Many researchers suggest that the climate of the early Earth was hot, but Kasting et al. (2006) argue that low values of $\delta^{18}O$ in sediments reflect different mid-ocean ridge depth and geothermal heat flux, not a hotter climate.

Another alternative focuses on how early Mars was kept warm; Segura et al. (2002) claim that impactors would have both delivered water vapor into the early Martian atmosphere, as well as released it from the crust. The authors assume that a 50-meter-deep global layer of water was needed to form the valley networks (Segura et al., 2002). This value is inconsistent with valley formation timescales, however. For example, continuous water flow for 10^3 to 10^4 years would have been needed to form the Parana

Basin valley networks (Barnhart et al., 2009). The proposition of episodic flood events by Segura et al. (2002) is inconsistent with such a timescale.

Other workers calculate that models of the changing solar luminosity are incorrect. Astronomers Wuchterl and Klessen (2001) simulate the star formation process, in order to predict the luminosity of the protostar that evolved to become our Sun. Their calculations predict that the protostar was 4 times as luminous as the Sun is today. So, perhaps the Sun started out much warmer than previously thought. Their model results and the implications come under scrutiny because the simulation is limited to the first few million years of formation, however (Schilling, 2001).

Chapter 2: Scattering and Absorption of Sunlight by Particles

Prior to running the photochemical model for the early Earth, we validated its output to ensure that its various routines were functioning properly. Observations of Saturn's largest moon Titan provide a ground truth of particle absorption. By replicating Titan's albedo spectrum we also validated the particle calculations of Haqq-Misra et al. (2008).

Hydrocarbon Aerosols in the Titan Photochemical Model

Initially, we assume a monodisperse particle size distribution (i.e. one particle size at each layer in the model). By adding a more realistic size distribution, the albedo spectrum can be replicated precisely. Previous photochemical models of Titan's atmosphere (e.g. Lavvas et al., 2003) assume various size distributions.

We define several parameters when characterizing absorption by particles, including the single scattering albedo, the extinction coefficient, the asymmetry parameter, and the size parameter. The single scattering albedo ω_0 is defined as

$$\omega_0 = \frac{\sigma_s}{\sigma_s + \sigma_a} \tag{6}$$

in which σ_s is the scattering cross section and σ_a is the absorption cross section. The extinction coefficient Q_{ext} is defined as

$$Q_{ext} = \frac{\sigma_e}{\pi r^2} \tag{7}$$

in which σ_e is the extinction cross section, defined as

$$\sigma_e = \sigma_a + \sigma_s \tag{8}$$

and r is the radius of the particle. The asymmetry parameter, g, is defined as

$$g = \int_0^{2\pi} \int_0^{\pi} P(\theta,\phi) \cos\theta \sin\theta d\theta d\phi \tag{9}$$

in which P is the phase function for scattering, θ is the angle between the incident light and the scattering direction, and φ is the azimuthal angle.

Finally, the size parameter x is defined as

$$x = \frac{2\pi r}{\lambda} \tag{10}$$

in which λ is the wavelength of the incident radiation.

According to Fig. 2, just longward of the Mie scattering regime ($x \sim 1$) and for a given imaginary index of refraction, the value of Q_{ext} increases. Logic then tells us that including smaller particles in our model should increase extinction.

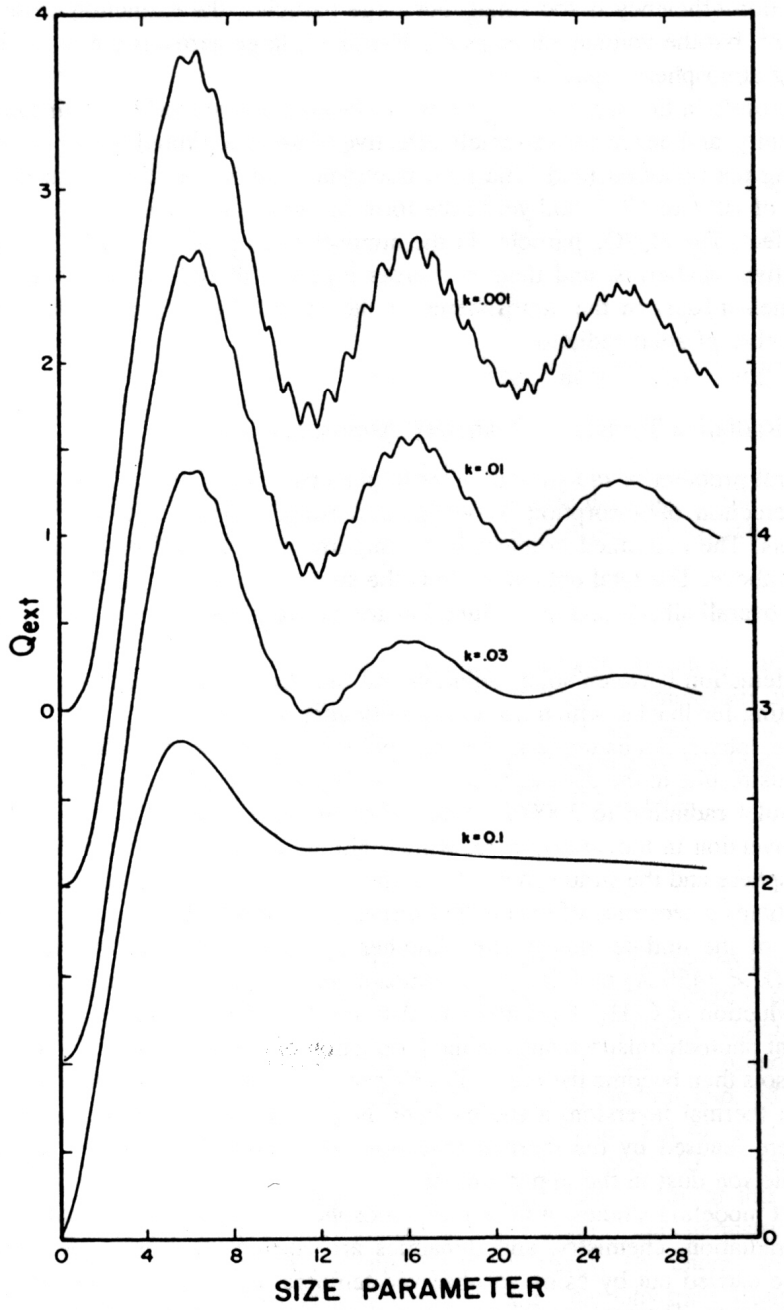

Fig. 2: Extinction efficiency versus size parameter, for a dielectric sphere with a real index of refraction of 1.33. The imaginary part, k, of the index of refraction is shown above the corresponding curves. Each curve has been moved up by 1 unit from the one below it. (Figure is taken from Yung and DeMore (1999), Figure 2.27.)

To include the effects of smaller particles in the photochemical model, we implemented a log-normal size distribution. The original number density of particles is divided among three bins, as shown Table 1. Note that the variables N_0 and R_0 are the original number density and particle radius, respectively, with a monodisperse particle size distribution. We also separately implemented a similar size distribution, but with five bins. Results of the output albedo spectrum are shown in Chapter 3.

Table 1: The number density of particles distributed among three size bins

Bin	**Number Density**	**Particle Radius**
1	$0.333N_0$	R_0
2	$0.333N_0(\frac{R_0}{R_2})^3$	$(\frac{R_0}{10})^{1/2}$
3	$0.333N_0(\frac{R_0}{R_3})^3$	$\frac{R_0}{10}$

Elemental Sulfur Aerosols (S_8) in the Early-Earth Photochemical Model

After this change to the Titan photochemical model, we turned our attention to determine if elemental sulfur aerosols (S_8) can help increase global surface temperatures on the early Earth. Previous research by Kasting et al. (1989) proves that S_8, a strong absorber in the near ultraviolet, could have formed an ultraviolet shield in an anoxic atmosphere. This layer is analogous to the modern ozone layer. Elemental sulfur is a prime candidate for forming such a shield because it is quite resistant to photochemical destruction and chemical attack. Elemental sulfur is also insoluble, so it would not be lost to the surface in large amounts (Kasting et al., 1989). The sources of sulfur in the early atmosphere are volcanoes and hot springs, which both emit gaseous SO_2 and H_2S (Walker and Brimblecombe, 1985). The majority of emissions of these two gases does not occur during eruption events, and so they constantly are being added to the atmosphere (Kasting et al., 1989). According to Kasting et al. (1989), elemental sulfur aerosols form from the photolysis of sulfur dioxide and the following subsequent reactions:

$SO_2 + h\nu \rightarrow SO + O$ (R1)
$SO + SO \rightarrow S + SO_2$ (R2)
$S + HCO \rightarrow HS + CO$ (R3)
$S + HS \rightarrow S_2 + H,$ (R4)
or , $S + S + M \rightarrow S_2 + M$ (R5)
$S_2 + S_2 + M \rightarrow S_4 + M$ (R6)
$S_4 + S_4 + M \rightarrow S_8$ (aerosol) + M (R7)

Here, hν is a photon and M is a third body that absorbs excess energy in a reaction. The authors note that S_8 also can form from photolysis of H_2S, but because SO_2 and H_2S

interconvert, the primary constituent is irrelevant (Kasting et al., 1989). In the more reduced atmosphere of the early Earth, S_8 aerosols would form more readily than they do today (Kasting et al., 1989). This result occurs because in the modern O_2-rich atmosphere, sulfur is readily oxidized to sulfate and sulfuric acid. If a layer of sulfur aerosols formed near the surface, then global temperatures could have been elevated.

To include the absorption by S_8 particles in the photochemical and climate models, we first had to derive optical properties of the particles, which vary with both the wavelength of incident radiation and the physical size of the aerosol.

Optical Properties for S_8 Particles

The data for the optical properties of S_8 come from two different sources. Sasson et al. (1985) measured the real index of refraction for liquid and solid sulfur in the range of 0.4 – 2 μm, along with the imaginary refractive index of liquid sulfur from 0.51 – 2 μm. We used the liquid sulfur values for both indices within this wavelength range.

At ultraviolet wavelengths (0.22 – 0.3 μm), Bass (1953) measured the optical density, or absorbance, A, of solid S_8 dissolved in ethyl alcohol. Absorbance is related to measured light intensity, I, by

$$I = I_0 10^{-A} \tag{11}$$

Here,

$$A = \frac{\varepsilon c d}{M} \tag{12}$$

where ε is the molar absorptivity, d is the path length [cm], c is the concentration [g/L], and M is the molecular weight. For a solid, c is equal to $10^3\rho$, where ρ is the density [g/cm^3]. The measured value of ε at 0.255 μm is $10^{3.6}$.

To convert this value into an imaginary refractive index, we first calculate the absorption cross section per molecule, σ. According to Beer's law,

$$I = I_0 e^{-\sigma n d} \tag{13}$$

where n is the number density [cm^{-3}]. By comparing expressions (11) and (13), and noting that $10^{-A} = e^{-\ln(10)A}$, we find that

$$\ln(10) A = \sigma n d \tag{14}$$

Now substitute (12) into (14), replacing the c with

$$c = 10^3 \rho = 10^3 n m_H M \tag{15}$$

where m_H is the mass of a hydrogen atom. This substitution yields

$$\sigma = \ln(10)\varepsilon 10^3 m_H \quad (16)$$

At 0.255 μm, we obtain $\sigma = 1.5*10^{-17}$ cm^{-2}, which is a reasonable cross section for a single S_8 molecule.

Finally, to calculate the imaginary refractive index, we define the absorption coefficient per unit mass, α', as

$$\alpha' = \sigma n \quad (17)$$

where $n = 3.87*10^{22}$ cm^{-3} is the number density of solid sulfur. The wavelength-dependent imaginary index of refraction is then

$$k(\lambda) = \frac{\alpha' \lambda}{4\pi} \quad (18)$$

where λ is the wavelength in cm. Calculated values of $k(\lambda)$ are plotted in Panel B of Fig. 3.

No data are available for S_8 absorption in the wavelength range 0.3 – 0.51 μm. Within this range, we used a log-linear interpolation between the calculated values of $k(\lambda)$ at each end of the range.

We also need the real index of refraction for S_8 at ultraviolet wavelengths. Not having any data for this quantity below 0.4 μm, we performed a visual extrapolation of the visible/near-infrared data (Fig. 3, Panel A). We arbitrarily picked a real refractive index of 3 at the shortest wavelength interval of our photochemical model, 0.12 μm, and then did a log-linear interpolation between this value and the tabulated value at 0.4 μm.

Calculation of Mie Scattering Parameters for S_8 Particles

The indices of refraction calculated above were used as input for a Mie scattering code (Mätzler, 2002). This code is based on algorithms developed in Bohren and Huffman (1983). Single scattering albedo ω_0, asymmetry parameter g, and extinction coefficient Q_{ext} were calculated for the relevant wavelength bins in both the photochemical and climate models and for 34 particle sizes ranging from 0.001 to 2 μm radius. Results for three different particle sizes are shown in Fig. 3, Panel C. These parameters were tabulated in files and used as lookup tables for the two codes. Note that absorption by S_8 shifts from ultraviolet to visible as the particle sizes become smaller.

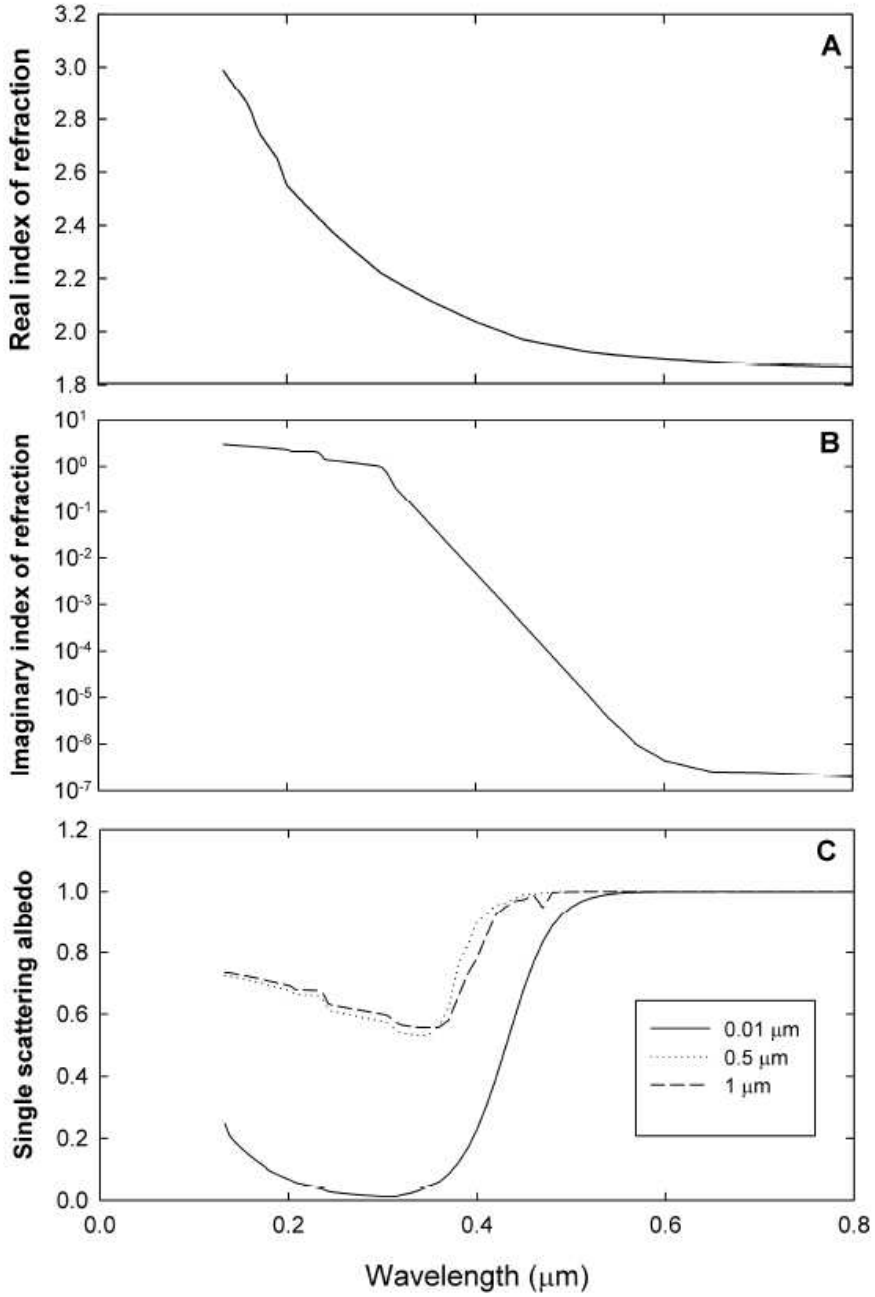

Fig. 3: (A) The real index of refraction and (B) the imaginary index of refraction of elemental sulfur input into the Mie scattering code of Mätzler (2002). (C) The single scattering albedo for three different particle sizes, as calculated by the Mie scattering code of Mätzler (2002).

Chapter 3: Modeling Titan's Atmosphere

Titan's geometric albedo spectrum, shown in Fig. 4, is calculated from observations by the Hubble space telescope and various other sources. The sharp slope in the albedo spectrum shortward of 850 nm is due to absorption by hydrocarbon aerosols created from the photolysis of methane. Using the photochemical model, we calculated the albedo spectrum shortward of 850 nm. Long-wavelength features are not of concern to us because they involve complex modeling of absorption by gases.

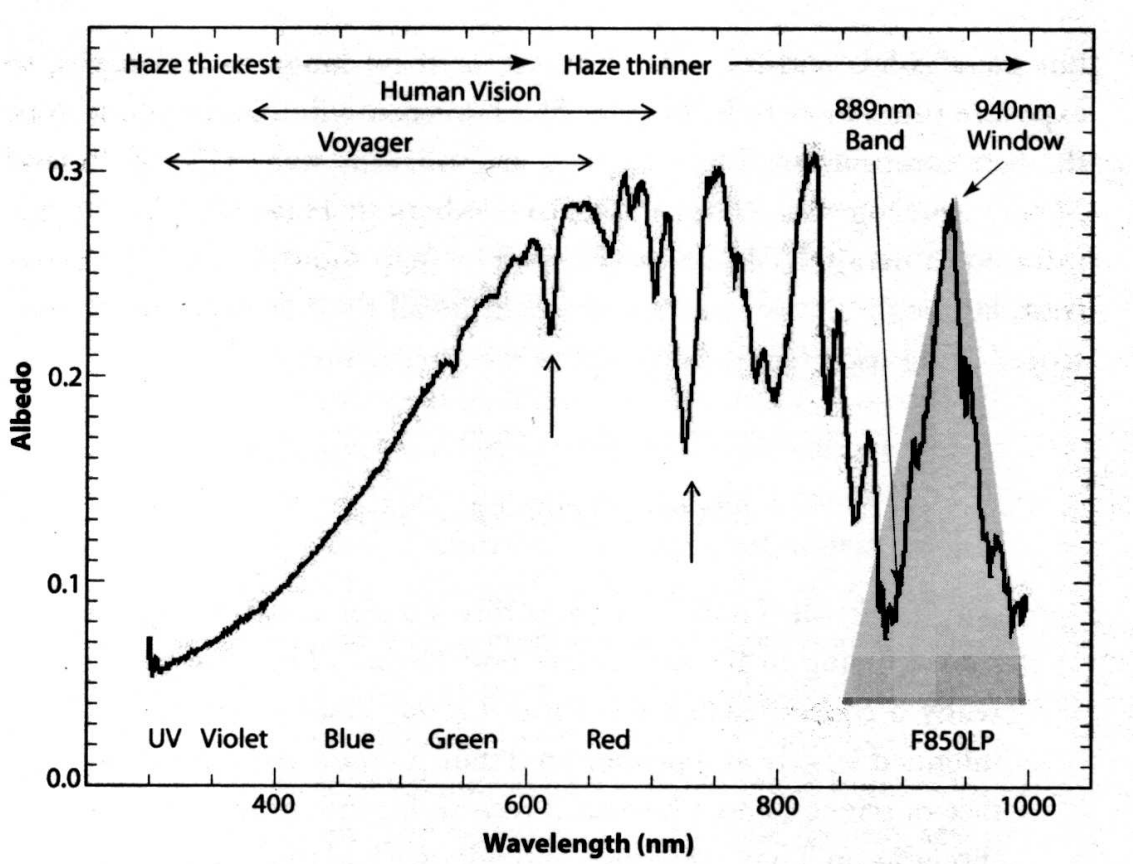

Fig. 4: Titan's albedo spectrum, derived from 1993 observations by Erich Karkoschka (Lorenz, personal communication, July 2009). Ref: Titan Unveiled, Fig 2.06. The vertical arrows indicate methane absorption features.

The Photochemical Model, Parameterized for Titan

The one-dimensional photochemical model used in these calculations was derived from the photochemical models of Pavlov et al. (2001) and Domagal-Goldman et al. (2008).

The photochemical model from which we started was adapted for early Earth conditions, with low O_2 levels due to the insignificance of photosynthesis. Chemical species in the photochemical code are long-lived, short-lived, or inert. These species participate in 359 reactions, shown in the appendix.

Mixing ratios for the long-lived species are calculated in a large, using the reverse Euler method, which requires setting up and inverting a large Jacobian matrix. The mixing ratios are calculated by solving

$$\frac{\partial f_i}{\partial t} = p_i - l_i n_i - \frac{\partial \phi_i}{\partial z} \tag{19}$$

Here, f_i is the mixing ratio of species i, n_i is total number density of species i, l_i is the chemical loss frequency of species i, p_i is the chemical production rate of species i, and φ_i is the flux of species i. In addition, mixing ratios for the short-lived species are calculated assuming steady-state conditions by:

$$n_i = \frac{p_i}{l_i} \tag{20}$$

Finally, the inert species are input into the photochemical model with a fixed mixing ratio profile.

In addition to the elemental sulfur aerosols, sulfate and hydrocarbon aerosols are also incorporated in the model. The Mie scattering parameters ω_0, Q_{ext}, and g for the hydrocarbon particles were calculated by Pavlov et al. (2001), and the Mie scattering parameters for the sulfate particles were calculated by Dr. Mark Claire, of the University of Washington. We assume a monodisperse particle size distribution for all three particles. The particles are subject to vertical transport, but their mixing ratios are calculated separately from the long-lived species, in a tridiagonal matrix. Time dependence is neglected for particles, but vertical transport is included. For the gaseous species, the partial differential equations used to determine the mixing ratios are solved using the reverse Euler method, which reverts to Newton's method when the time step is sufficiently large. Newton's method often is used in numerical analysis. Newton's method begins with an initial guess for the root of an equation, and then subsequent time steps iteratively converge on the solution.

The photochemical model with which we began was parameterized for conditions on the early Earth. In order to simulate Titan, we first had to change the entire chemical scheme. Titan's atmosphere consists of 1.6% CH_4 and 98.4% N_2 (Niemann et al., 2005), as well as some trace gases. Titan's atmosphere contains almost no atmospheric O_2 or sulfur-bearing species. Therefore, we removed chemical reactions that included oxygen and sulfur (including both sulfur and sulfate aerosols). More detailed photochemical models incorporate various other species (e.g. Lavvas et al., 2007), but here all oxygen-containing species were removed because they are scarce. The chemical reactions included in our model are shown in the appendix.

In addition to editing the chemical scheme, we also edited the values of basic planetary parameters. A comparison of these parameters with that of the present-day Earth parameters is shown in Table 2. For Titan, the gravitational acceleration comes from Wikipedia, the surface albedo value comes from Gibbard et al. (2004), the tropopause height comes from Courtin et al. (2002), the surface pressure comes from Tyler et al. (1981), and the planetary radius comes from solarsystem.nasa.gov.

Table 2: Comparison of several planetary parameter values for the Earth and Titan.

	Earth	Titan
Gravitational Acceleration	9.807 m/s^2	1.352 m/s^2
Solar flux (scaled to Earth)	1	0.011
Surface Albedo	0.25	0.1
Height of each atmospheric layer in photochemical code	1 km	5 km
Tropopause height	11 km	30 km
Surface Pressure	1 bar	1.6 bar
Planetary Radius	$6.37*10^6$ m	$2.575*10^6$ m

Two other differences between Earth and Titan are the atmospheric temperature profile and the eddy-diffusion profile. In our model, the eddy-diffusion coefficient characterizes mixing within the lower atmosphere. We used the eddy-diffusion profile of Yung et al. (1984), as presented in Toublanc et al. (1995). This profile is presented in Fig. 5, Panel B. Additionally, we used data from Courtin et al. (2002) to create the vertical temperature profile shown in Fig. 5, Panel A. This profile compares well with the vertical temperature profile from the Huygens Atmospheric Structure Instrument (HASI), as shown in Lavvas et al. (2007).

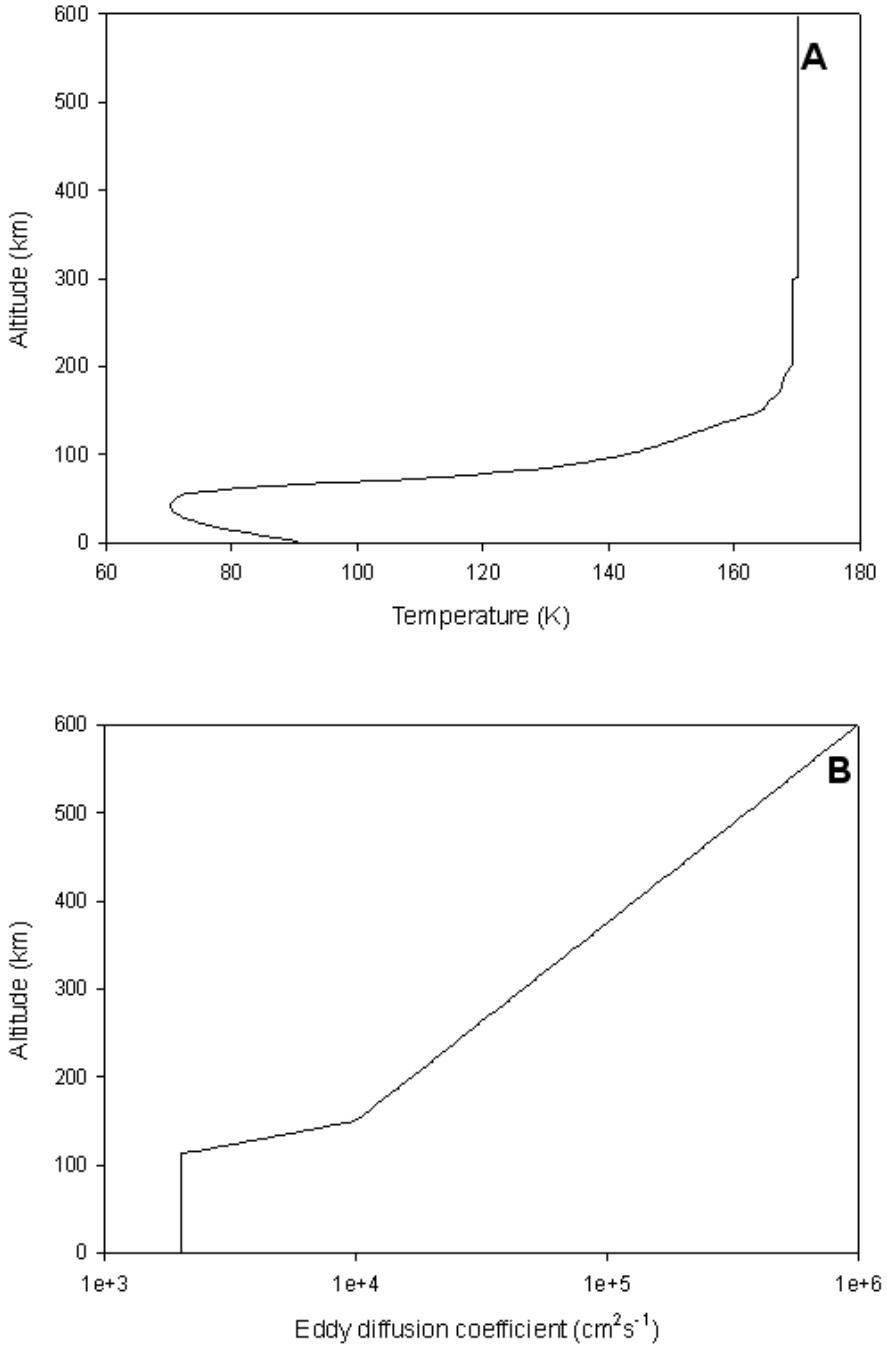

Fig. 5: Panel A shows the vertical temperature profile used in our Titan photochemical model. Panel B shows the eddy-diffusion coefficient profile used in our photochemical model.

Methane photolysis was of primary interest to us here, and so we strove to represent methane accurately in the model. Methane on Titan is analogous to water on Earth, in that both constituents drive the hydrological cycle on the respective planetary bodies. Workers hypothesize radar observations of dark patches on Titan are lakes

composed of various hydrocarbons (Courdier et al., 2009). Additionally, recent observations from ground telescopes revealed clouds in the atmosphere (Tokano et al., 2006).

We collected key information about the phase changes of methane from the NIST webbook (http://webbook.nist.gov/cgi/cbook.cgi?Name=methane&Units=SI&cTP=on). These data are shown in Table 3.

Table 3: Thermodynamic data for methane

Measured Parameter	Value
T_{triple}	90.67 K
P_{triple}	0.1169 bars
ΔH_{vap}	8.519 kJ/mol[1]
ΔH_{sub}	9.7 kJ/mol[2]
[1] Vogt and Pitzer (1976) [2] Stephenson and Malanowski (1987)	

The next step was to calculate the saturation vapor pressure of methane in each layer in the atmosphere. First, we solved the Clausius-Clapeyron equation

$$e_j = p_0 \exp\left[\frac{\Delta H_j}{R}\left(\frac{1}{T_0} - \frac{1}{T_j}\right)\right] \tag{21}$$

where e_j is the saturation vapor pressure of methane at level j, p_0 is the triple point pressure, ΔH_j is the enthalpy of vaporization or sublimation (the former if the temperature of the layer is greater than the triple point temperature and the latter if the temperature of the layer is less than the triple point temperature), R is the universal gas constant (8.314 $JK^{-1}mol^{-1}$), T_0 is the triple point temperature, and T_j is the temperature at level j.

Then, we calculated the pressure at each level using the ideal gas law

$$p_j = \frac{\rho_j k T_j}{m_j} \tag{22}$$

Here, p_j is the pressure at level j, ρ_j is the atmospheric number density at level j ($area^{-3}$), k is Boltzmann's constant, and m_j is the mass of species j.

Next, the saturation mixing ratio of methane at each level is found from

$$e_{CH4,j} = \frac{e_j}{p_j} \tag{23}$$

Finally, the methane relative humidity profile was calculated from in-situ measurements made with the Gas Chromatograph Mass Spectrometer instrument aboard the Huygens probe (Graves et al., 2008), and is shown below in Fig. 6.

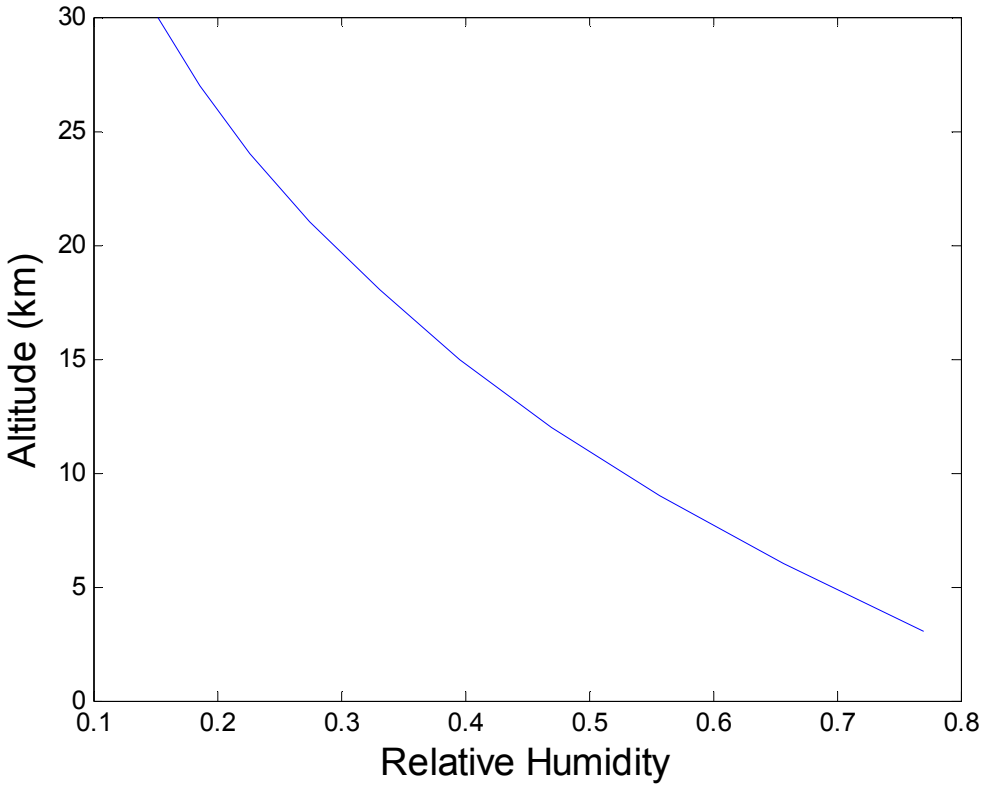

Fig. 6 : The tropospheric relative humidity profile adopted in the model.

In our model, we calculate the methane concentration in the troposphere from

$$[CH_4] = RH_j e_{CH4,j} \tag{24}$$

where $[CH_4]$ is the methane mixing ratio and RH_j is the methane relative humidity at level j.

Above the troposphere height of 30 km (Courtin et al., 2002), we assume a constant CH_4 mixing ratio of 1.6%. The saturation mixing ratio and actual calculated mixing ratio of methane are shown in Fig. 7.

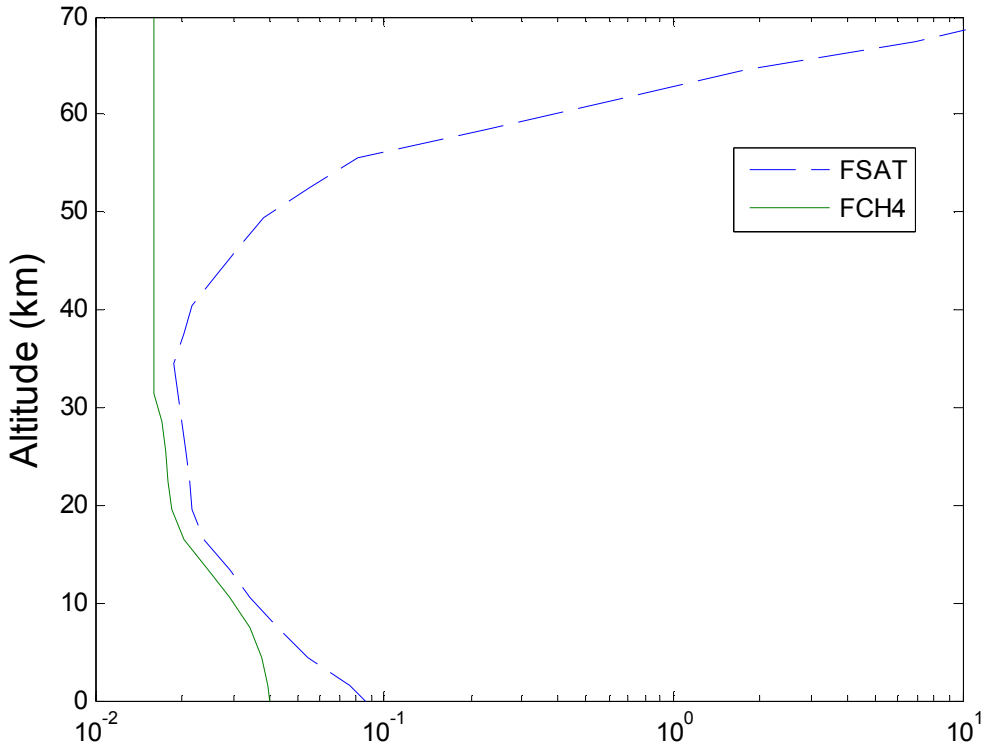

Fig. 7: Lower tropospheric profiles of the saturation mixing ratio of CH_4 (FSAT) and the mixing ratio of CH_4 (FCH4), as calculated in the photochemical model.

Edits to the Photochemical Code

We discovered two potential problems with the model. First, the two-stream code, modeled after the two-stream radiative transfer code of Toon et al. (1989) had a slight error in one of its calculations. The particle optical depth was being calculated in such a way that only contributions from the last listed particle were considered. A small change to the programming logic fixed this problem.

Also, we improved the consistency of the two-stream radiative transfer code by calculating absorption in the far-UV region (1216 Å - 1725 Å) for the following gases: H_2S, NH_3, O_3, H_2O, SO_2, O_2, and CO_2. Cross sections of H_2O, SO_2, O_2, and CO_2 were already included in the code. We obtained the UV absorption cross sections for H_2S, NH_3, and O_3 from the website of the NASA Astrobiology-affiliated Virtual Planetary Laboratory (http://vpl.astro.washington.edu).

Replicating Titan's Albedo Spectrum

Having changed the model's chemistry, temperature profile, eddy-diffusion profile, and hydrologic cycle, we ran the photochemical model and compared the output albedo spectrum with the observed albedo spectrum (Fig. 8). The albedo spectrum calculated from the photochemical model is shown in Fig. 7. The slopes of the two spectra match well shortward of 600 nm match well.

Figure 8 also shows the albedo spectrum produced with these smaller particles included. Inclusion of smaller particles shifts the spectrum slightly and eliminates the upturn in the spectrum at shorter wavelengths, and so it definitely provides a better fit to observations than does the monodisperse size distribution.

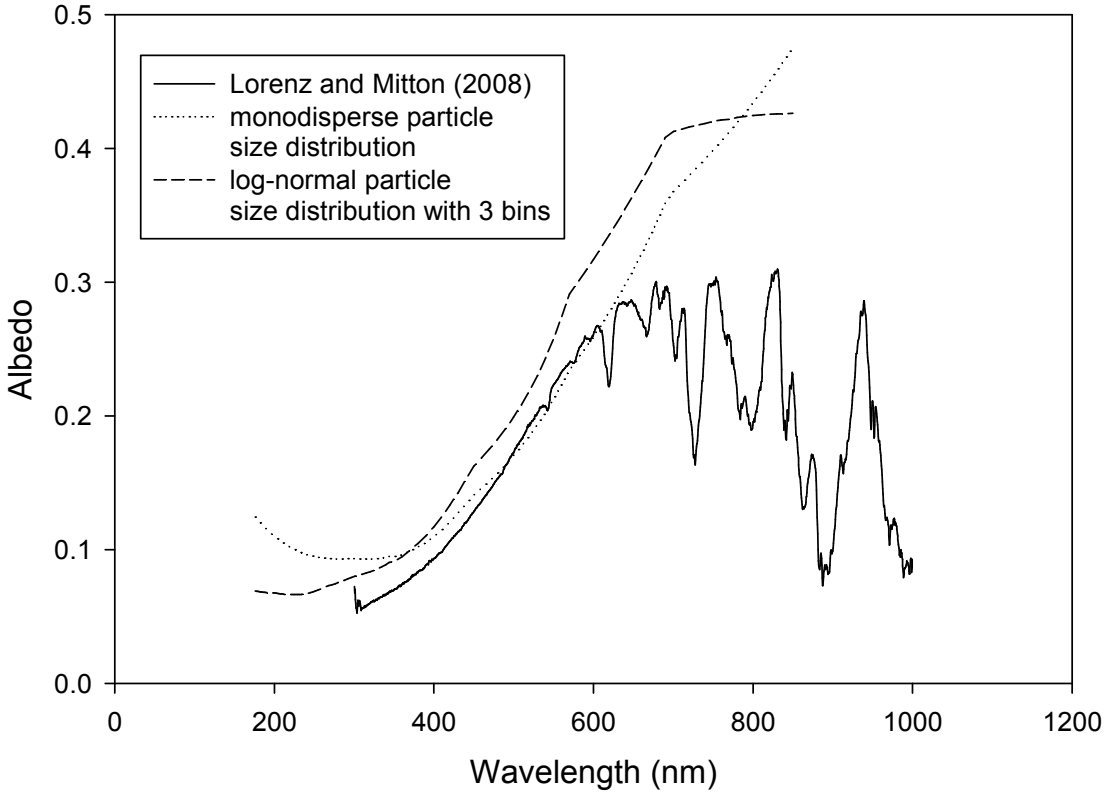

Fig. 8: Albedo spectra calculated in the photochemical model, plotted with the spectrum from Figure 4.

Validation of the photochemical code was successful. Additionally, we demonstrated that we are able to create a particle size distribution and investigate the effects of a changing distribution on the geometric albedo spectrum. This method may be especially useful in the future, when and if the particle size distribution is better constrained because of more in-situ measurements.

Chapter 4: Modeling the early Earth's Atmosphere

With the optical properties of S_8 particles already calculated, we took two final steps to set the photochemical model up to include sulfur aerosols. First, the chemical scheme was changed to represent conditions on the early Earth. A list of the 359 chemical reactions can be found in the Appendix. Second, we optimized conditions for maximum buildup of sulfur particles. Ono et al. (2003) varied the amount of sulfur particles produced by altering the SO_2 input from volcanic outgassing. In their model, the maximum buildup of S_8 particles relative to sulfate and hydrocarbon particles occurs with an SO_2 outgassing rate of $3.5*10^9$ $cm^{-2}s^{-1}$, which is approximately three times the present outgassing rate. We used this rate as a starting point in my calculations.

In addition to the outgassing rate, we altered two other parameters in the code. First, we eliminated SO_2 rainout from the atmosphere. This step follows the methods of Kasting et al. (1989) by making the special assumption that the ocean was saturated with SO_2. This assumption may or may not have been the case in reality, but it maximizes the abundance of S_8 in the atmosphere. Second, we eliminated surface deposition of H_2. Molecular hydrogen is consumed by methanogens via

$$CO_2 + 4H_2 \rightarrow CH_4 + 2H_2O \qquad \text{(R8)}$$

Hence, the model neglects this biologic cycle, minimizing the number of variables in the calculations. We implemented both of these conditions separately and together, while varying the SO_2 outgassing rate.

In order to increase the optical depth of the S_8 particles to an amount comparable to the sulfate optical depth, we had to increase the sulfur outgassing rate to $3.5*10^{10}$ atoms $cm^{-2}s^{-1}$, which is 35 times the current total surface sulfur flux of $1*10^9$ atoms $cm^{-2}s^{-1}$, which includes both H_2S and SO_2 emissions. A more detailed description of the treatment of sulfur within the model can be found in Kasting et al. (1989).

Results from the simulations are given in Table 4. Case A is the simulation with a SO_2 outgassing rate of $3.5*10^9$ $cm^{-2}s^{-1}$, and Case B is Case A without sulfur rainout and H_2 surface deposition. As shown in Table 4, the extinction of optical depth for S_8 particles increases directly in proportion to the SO_2 outgassing rate. The elimination of H_2 deposition and SO_2 rainout both cause the optical depth for S_8 particles to increase, as well. Note that the methane concentration is held at a constant 50 ppmv to reduce the formation of hydrocarbon aerosols that cool the surface.

Table 4: Data from various runs of the photochemical model.

	Case A: SO_2 outgassing rate = $3.5 * 10^9$ $cm^{-2}s^{-1}$	**Case A with no sulfur rainout**	**Case A with no H_2 surface deposition**	**Case B: Case A with no sulfur rainout and no H_2 surface deposition**	**Case B with a SO_2 outgassing = $1.0 * 10^{10}$ $cm^{-2}s^{-1}$**	**Case B with a SO_2 outgassing rate = $3.5 * 10^{10}$ $cm^{-2}s^{-1}$**
Mixing Ratio (bars)						
CO_2	$3.10 * 10^{-2}$	$3.10*10^{-2}$	$3.10*10^{-2}$	$3.10*10^{-2}$	$3.10*10^{-2}$	$3.10*10^{-2}$
CH_4	$5.00 * 10^{-5}$	$5.00*10^{-5}$	$5.00*10^{-5}$	$5.00*10^{-5}$	$5.00*10^{-5}$	$5.00*10^{-5}$
H_2	$1.85 * 10^{-5}$	$1.83*10^{-5}$	$9.86*10^{-4}$	$9.74*10^{-4}$	$7.98*10^{-4}$	$3.89*10^{-4}$
CO_2	$3.91 * 10^{-6}$	$3.93*10^{-6}$	$1.69*10^{-5}$	$1.69*10^{-5}$	$1.54*10^{-5}$	$1.01*10^{-5}$
SO_2	$8.63 * 10^{-12}$	$1.36*10^{-11}$	$6.25*10^{-12}$	$9.45*10^{-12}$	$3.15*10^{-11}$	$2.89*10^{-10}$
Sulfur Column Depth (cm)						
H_2S	$2.31*10^{15}$	$2.44*10^{15}$	$4.20*10^{15}$	$4.40*10^{15}$	$5.78*10^{15}$	$6.85*10^{15}$
SO_2	$4.10*10^{15}$	$4.33*10^{15}$	$3.93*10^{15}$	$4.06*10^{15}$	$8.40*10^{15}$	$3.24*10^{16}$
Extinction Optical Depths at 500 nm						
SO_4	$1.06*10^{-1}$	$1.10*10^{-1}$	$8.27*10^{-2}$	$8.52*10^{-2}$	$1.64*10^{-1}$	$4.62*10^{-2}$
S_8	$8.40*10^{-3}$	$1.01*10^{-2}$	$1.30*10^{-2}$	$1.47*10^{-2}$	$6.39*10^{-2}$	$2.08*10^{-1}$
Hydrocarbons	$1.40*10^{-13}$	$1.43*10^{-13}$	$6.46*10^{-14}$	$6.50*10^{-14}$	$7.14*10^{-14}$	$1.89*10^{-13}$

The Climate Model

The climate model used here is derived from the model used by both Pavlov et al. (2001) and Haqq-Misra et al. (2008). It is a one-dimensional, cloud-free, radiative-convective climate model. Output of a vertical temperature profile is computed from an initial pressure-temperature profile and a value for the solar constant. In our calculations, the solar constant was taken to be 0.8, an estimate that is valid for the Late Archean/ Paleoproterozoic. The radiative transfer code is based on the delta two-stream code of Toon et al. (1989). Absorption of solar radiation by O_3, CO_2, O_2, H_2O, and CH_4 is parameterized using four-term correlated k-coefficients. For these calculations, the atmosphere is divided into 100 vertical levels. The local temperature change in each layer is calculated by solving

$$\frac{\partial T}{\partial t} = \frac{-g}{c_p}\frac{\partial F}{\partial P} \tag{25}$$

where T is temperature, t is time, g is the gravitational constant, c_p is the specific heat capacity at constant pressure, F is flux, and P is pressure.

Fluxes are defined at the layer boundaries, and temperature is defined at the layer midpoints. Radiative fluxes are modeled explicitly. Convective fluxes also are modeled, but implicitly through *convective adjustment*. When the lapse rate exceeds the moist adiabatic lapse rate (~6 K/km at Earth's surface), *convective adjustment* reduces the lapse rate accordingly. Time-independent, globally averaged calculations, such as the ones here, often parameterize convection in this manner. Below the troposphere, the relative humidity follows the profile designated by Manabe and Wetherald (1967).

Results from the Climate Model

Vertical profiles of the S_8 and sulfate aerosol radii and number density were produced by the photochemical model and were used as lookup tables in the climate model. We ran the climate model four times, altering the particles included in the calculations. In the first simulation, we completely excluded particles, so as to isolate the effect of gaseous absorption. In the second run, we included only sulfate particles. In the third run, we included only elemental sulfur particles, and in the fourth and final run, we included both sulfate and sulfur particles.

Mixing ratios of long-lived chemical species were not incorporated from the photochemical model; rather, we assumed a 1-bar atmosphere composed of only N_2 (volume mixing ratio of 0.97) and CO_2 (volume mixing ratio of 0.03). Other 1-D models for the Late Archean/Paleoproterozoic incorporate CH_4 and higher-order hydrocarbons (Haqq-Misra et al., 2008). For our calculations here, we wish to isolate the warming effect of the sulfur particles, and so the possible incompleteness of our atmosphere is not of concern.

For the simulation with no particles included, the calculated surface temperature, 283.7 K, is slightly higher than the value calculated by Haqq-Misra et al. (2008) under the same conditions, 278 K. Both of these values are for a methane mixing ratio of zero and a CO_2 partial pressure of 0.03 bar. Although we both use the same climate model,

Haqq-Misra et al. (2008) has only 25 vertical layers in their model, whereas our calculations are done with 100 vertical layers. Within the climate model, increasing the number of vertical layers, especially in atmospheres with steep tropospheric temperature gradients, can increase the surface temperature by around 10 K. When only sulfate particles are added, the surface temperature decreases to 278.9 K. When only sulfur particles are included, the surface temperature was 281.0 K, and last when both sulfur and sulfate particles are included, the surface temperature is 276.9 K. Temperature profiles for the four cases are shown in Fig. 9.

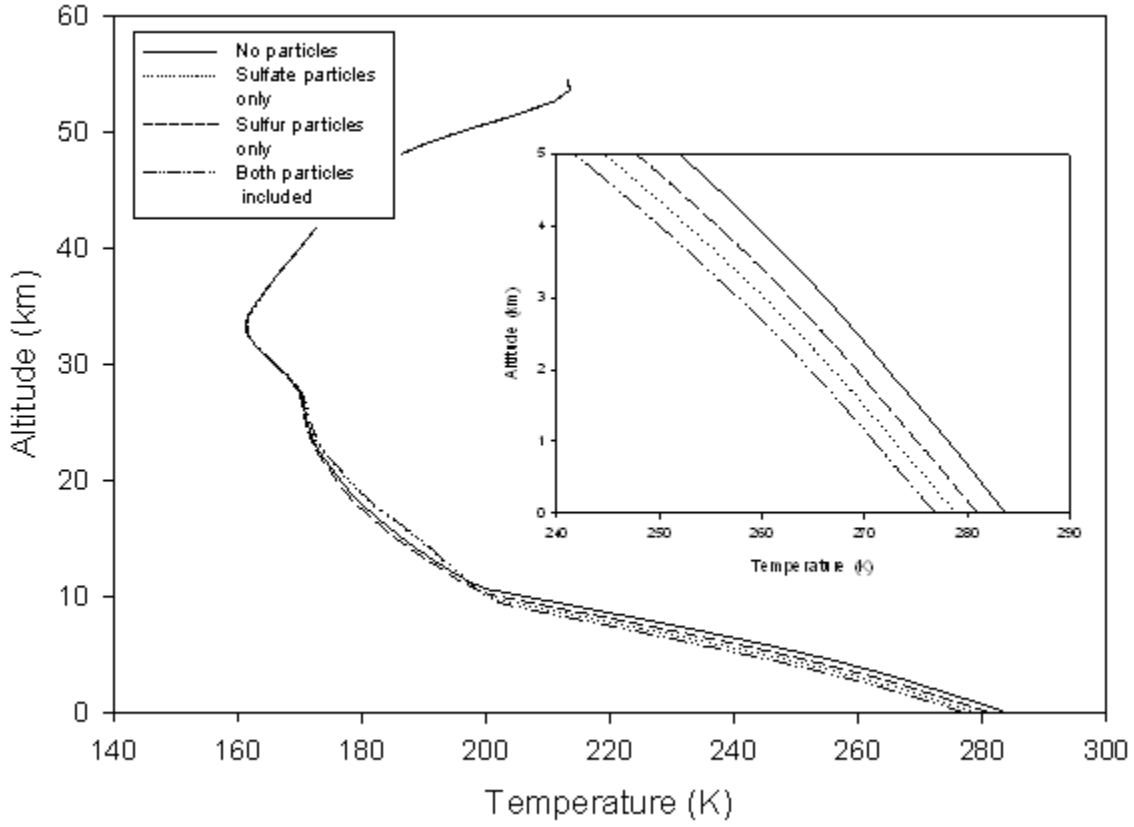

Fig. 9: Vertical temperature profiles produced from the climate model. The inset graph is the lowest 5 km of the larger graph.

Chapter 5: Discussion and Conclusion

In conclusion, elemental sulfur particles are ineffective at increasing surface temperatures. Inclusion of elemental sulfur particles in a one-dimensional radiative convective climate model lowers the surface temperature by 2.6 K. Additionally, the combination of sulfate aerosols and elemental sulfur aerosols also lowers the surface temperature. Concurrent investigation of absorption by S_8 particles by Tian et al. (in press) verifies that S_8 particles cause surface cooling. As Fig. 3 shows, larger particles have higher single-scattering albedos shortward of 0.4 μm, and therefore smaller particles are more effective absorbers. An interesting investigation would be to create a distribution of sulfur particle sizes with the majority of the particles having a radius smaller than 0.01 μm. Perhaps the surface would warm, rather than cool.

Additionally, it may be possible to warm the surface with amorphous sulfur particles (S_3 and S_4). Amorphous sulfur is thought to absorb UV radiation in the clouds of Venus (Toon et al., 1982). By calculating optical properties for amorphous sulfur, such particles could be included in the photochemical and climate models.

Subsequent research will allow scientists to refine the definition of a habitable planet, and it will guide our search for habitable extrasolar planets and life elsewhere in the universe.

REFERENCES

Barnhart C.J., Howard A.D., & Moore J.M. (2009). Long-term precipitation and late-stage valley network formation: Landform simulations of Parana Basin, Mars. *Journal of Geophysical Research-Planets* 114

Bass, A.M. (1953). The optical absorption of sulfur. *Journal of Chemical Physics, 21*(1), 80-82.

Bohren, C.F., Huffman, R.D. (1983). *Absorption and Scattering of Light by Small Particles.* New York, New York: John Wiley & Sons, Inc.

Cordier, D., Mousis, L., Lunine, J.I., et al (2009). An estimate of the chemical composition of Titan's lakes. *Astrophysical Journal Letters, 707*(2), 128-131.

Courtin, R., Kim, S.J. (2002). Mapping of Titan's tropopause and surface temperatures from Voyager IRIS spectra. *Planetary and Space Science, 50*(3), 309-321.

Dlugokencky, E.J., Houweling, S., Bruhwiler, L., et al. (2003). Atmospheric methane levels off: temporary pause or a new steady-state? *Geophysical Research Letters, 30*(19).

Domagal-Goldman, S.D., Kasting, J.F., Johnston, D.T., et al. (2008). Organic haze, glaciations and multiple sulfur isotopes in the mid-Archean era. *Earth and Planetary Science Letters, 269*(1-2), 29-40

Gibbard, S.G., Macintosh, B., Gavel, D., et al. (2004). Speckle imaging of Titan at 2 microns: surface albedo, haze optical depth, and tropospheric clouds 1996 – 1998/ *Icarus,* 169(2), 429 – 439.

Gough, D.O. (1981). Solar Interior Structure and Luminosity Variations. *Solar Physics, 74*(1), 21-34.

Graves, S.D.B., McKay, C.P., Griffith, C.A., et al. (2008). Rain and hail can reach the surface of Titan. *Planetary and Space Science, 56*(3-4), 346-357.

Haqq-Misra, J.D., Domagal-Goldman, S.D., Kasting, P.J., & Kasting, J.F. (2008). A Revised, Hazy Methane Greenhouse for the Early Earth. *Astrobiology,8*(6), 1127-1137.

Haselgrove, C.B., Hoyle, F. (1959). Main-sequence stars. *Monthly Notices of the Royal Astronomical Society, 119*(2), 112-123.

Hoyle, F., Wilson, O.C. (1958). Some theoretical aspects of H and K emission in late-type stars. *Astrophysical Journal,128*(3), 604-615.

Kasting, J.F., Pollack, J.B., Pollack, J.B., & Crisp, D. (1984). Effects of high CO_2 levels on surface-temperature and atmospheric oxidation-state of the early Earth. *Journal of Atmospheric Chemistry,1*(4), 403-428.

Kasting, J.F., Toon, O.B., & Pollack, J.B. (1988). How Climate Evolved on the Terrestrial Planets. *Scientific American*, *256*, 90-97.

Kasting, J.F., Zahnle, K.J., Pinto, J.P., & Young, A.T. (1989). Sulfur, ultraviolet radiation, and the early evolution of life. *Origins of Life and Evolution of the Biosphere, 19*(2), 95-108.

Kasting, J.F. (1997). *Science, 276*(5316), 1213-1215.

Kasting, J.F., Howard, M.T., Wallmann, K., et al. (2006). Paleoclimates, ocean depth, and the oxygen isotopic composition of seawater. *Earth and Planetary Science Letters, 252*(1-2), 82 – 93.

Kasting, J.F. (2009). *How to Find a Habitable Planet.* Princeton, New Jersey: Princeton University Press.

Lavvas, P.P., Coustenis, A., Vardavas, I.M. (2008). Coupling photochemistry with haze formation in Titan's atmosphere, part 1: Model description. *Planetary and Space Science, 56*(1), 27 – 66.

Lavvas, P.P., Coustenis, A., & Vardavas, I.M. (2008). Coupling photochemistry with haze formation in Titan's atmosphere, Part II: Results and validation with Cassini/Huygens data. *Planetary and Space Science, 56*(1), 67-99.

Lorenz, R., Mitton, J. (2008). *Titan Unveiled.* Princeton, New Jersey: Princeton University Press.

Lunine, J.I. (2005). *Astrobiology: A Multidisciplinary Approach.* San Francisco, California: Addison Wesley.

Manabe, S., Wetheral, R.T. (1967). Thermal equilibrium of atmosphere with a given distribution of relative humidity. *Journal of Atmospheric Sciences, 24*(3), 241-259.

Mätzler, C. MATLAB Functions for Mie Scattering and Absorption, code available at: http://diogenes.iwt.uni-bremen.de/vt/laser/wriedt/Mie_Type_Codes/body_mie_type_codes.html

McKay, C.P., Pollack, J.B., & Courtin, R. (1991). The greenhouse and antigreenhouse effects on Titan. *Science, 253*(5024), 1118-1121.

Niemann, H.B., Atreya, S.K., Bauer, S.J., et al. (2005). The abundances of constituents of Titan's atmosphere from the GCMS instrument on the Huygens probe. *Nature, 438*(7069), 779-784.

National Institute of Standards and Technology, Chemistry Webbook. *Methane.* Retrieved from http://webbook.nist.gov/cgi/cbook.cgi?Name=methane&Units=SI&cTP=on.

Ono, S., Eigenbrode, J.L., Pavlov, A.A., et al. (2003). New insights into Archean sulfur cycle from mass-independent sulfur isotope records from the Hamersley Basin, Australia. *Earth and Planetary Science Letters, 213*(1-2), 15-30.

Pavlov, A.A., Kasting, J.F., Brown, L.L., et al. (2000). Greenhouse warming by CH_4 in the atmosphere of the early Earth. *Journal of Geophysical Research- Planets, 105*(E5), 11981 – 11990.

Pavlov, A.A., Brown, L.L., & Kasting, J.F. (2001). UV shielding of NH_3 and O_2 by organic hazes in the Archean atmosphere. *Journal of Geophysical Research – Planets, 106*(E10), 23267-23287.

Raymond, S.N., Quinn, T., & Lunine, J.I. (2006). High-resolution simulations of the final assembly of Earth-like planets I. Terrestrial accretion and dynamics. *Icarus, 183*(2), 265-282.

Rondanelli, R., Lindzen, R.S. (2010). Can cirrus clouds in the tropics provide a solution to the faint young Sun paradox? *Journal of Geophysical Research, 115*, D02108.

Rosing, M.T., Bird, D.K., Sleep, N.H., et. al. (2010). No climate paradox under the faint early Sun. *Nature, 464,* 744 – 747.

Rye, R., Kuo, P.H., & Holland, H.D. (1995). Atmospheric carbon dioxide concentrations before 2.2 billion years ago. *Nature*, *378*(6557), 603–605.

Sagan, C., Mullen, G. (1972). Earth and Mars: Evolution of Atmospheres and Surface Temperatures. *Science, 177*(4043), 52-56.

Sasson, R., Wright, R., Arakawa, E.T., et al. (1985). Optical-properties of solid and liquid sulfur at visible and infrared wavelengths. *Icarus, 64*(3).

Schilling, G. (2001). Astrophysics: New model shows Sun was a hot young star. *Science, 293*(5538), 2188-2189.

Segura, T.L., Toon, O.B., Colaprete, A., et al. (2002). Environmental effects of large impacts on Mars. *Science, 298*(5600), 1977-1980.

Solarsystem.nasa.gov

Stephenson, R.M., Malanowski, S. (1987). *Handbook of the Thermodynamics of Organic Compounds.* New York, New York: Elsevier.

Tian, F., Claire, M.W., Haqq-Misra, J.D., et al. (2009). Photochemical and climate consequences of sulfur outgassing on early Mars. *Submitted for publication.*

Titan (moon). On *wikipedia*. Retrieved from http://www.wikipedia.com.

Tokano, T., McKay, C.P., Neubauer, F.M., et al. (2006). Methane drizzle on Titan. *Nature, 442*(7101), 432 – 435.

Toon, O.B., Turco, R.P., & Pollack, J.B. (1982). The Ultraviolet Absorber on Venus: Amorphous Sulfur. *Icarus, 51*(2), 358-373.

Toon, O.B., McKay, C.P., Ackerman, T.P., et al. (1989). Rapid calculation of radiative heating rates and photodissociation rates in inhomogeneous multiple-scattering atmospheres. *Journal of Geophysical Research- Atmospheres, 94*(D13), 16287 – 16301.

Toublanc, D., Parisot, J.P., Brillet, J., et al. (1995). Photochemical modeling of Titan's atmosphere. *Icarus, 113*(1), 2-26.

Tyler, G.L., Eshleman, V.R., Anderson, J.D., et al. (1981). Radio science investigations of the Saturn system with Voyager 1: Preliminary results. *Science, 212*(4491), 201-206.

Virtual Planetary Laboratory. *Ultraviolet cross sections*. Retrieved from vpl.astro.washington.edu.

Vogt, G.J., Pitzer, K.S. (1976). Entropy and heat capacity of methane, spin-species conversion. *Journal of Chemical Thermodynamics, 8*(11), 1011-1031.

Wuchterl, G., Klessen, R.S. (2001). The first million years of the Sun: a calculation of the formation and early evolution of a solar mass star. *Astrophysical Journal,560*(2), L185-L188.

Yung, Y.L., Allen, M., & Pinto, J.P. (1984). Photochemistry of the atmosphere of Titan – comparison between model and observations. *Astrophysical Journal Supplement Series, 55*(3), 465 – 506.

Yung, Y.L., DeMore, W.B. (1998). *Photochemistry of Planetary Atmospheres.* New York, New York: Oxford University Press.

APPENDIX

Chemical Reactions in the Photochemical Model, Parameterized for the Early Earth

Reaction Number	
1	$H_2O + O(^1D) = 2OH$
2	$H_2 + O(^1D) = OH + H$
3	$H_2 + O = OH + H$
4	$H_2 + OH = H_2O + H$
5	$H + O_3 = OH + O_2$
6	$H + O_2 + M = HO_2 + M$
7	$H + HO_2 = H_2 + O_2$
8	$H + HO_2 = H_2O + O$
9	$H + HO_2 = OH + OH$
10	$OH + O = H + O_2$
11	$OH + HO_2 = H_2O + O_2$
12	$OH + O_3 = HO_2 + O_2$
13	$HO_2 + O = OH + O_2$
14	$HO_2 + O_3 = OH + {}_2O_2$
15	$HO_2 + HO_2 = H_2O_2 + O_2$
16	$H_2O_2 + OH = HO_2 + H_2O$
17	$O + O + M = O_2 + M$
18	$O + O_2 + M = O_3 + M$
19	$O + O_3 = 2O_2$
20	$OH + OH = H_2O + O$
21	$O(^1D) + M = O(^3P) + M$
22	$O(^1D) + O_2 = O(^3P) + O_2$
23	$O_2 + hv = O(^3P) + O(^1D)$
24	$O_2 + hv = O(^3P) + O(^3P)$
25	$H_2O + hv = H + OH$
26	$O_3 + hv = O_2 + O(1D)$
27	$O_3 + hv = O_2 + O(^3P)$
28	$H_2O_2 + hv = 2OH$
29	$CO_2 + hv = CO + O(^3P)$
30	$CO + OH = CO_2 + H$
31	$CO + O + M = CO_2 + M$
32	$H + CO + M = HCO + M$
33	$H + HCO = H_2 + CO$
34	$HCO + HCO = H_2CO + CO$
35	$OH + HCO = H_2O + CO$
36	$O + HCO = H + CO_2$
37	$O + HCO = OH + CO$
38	$H_2CO + hv = H_2 + CO$
39	$H_2CO + hv = HCO + H$

40	$HCO + hv = H + CO$
41	$H_2CO + H = H_2 + HCO$
42	$CO_2 + hv = CO + O(^1D)$
43	$H + H + M = H_2 + M$
44	$HCO + O_2 = HO_2 + CO$
45	$H_2CO + OH = H_2O + HCO$
46	$H + OH + M = H_2O + M$
47	$OH + OH + M = H_2O_2 + M$
48	$H_2CO + O = HCO + OH$
49	$H_2O_2 + O = OH + HO_2$
50	$HO_2 + hv = OH + O$
51	$CH_4 + hv = 1CH_2 + H_2$
52	$C_2H_6 + hv = 2\ ^3CH_2 + H_2$
53	$C_2H_6 + hv = CH_4 + {}^1CH_2$
54	$HNO_2 + hv = NO + OH$
55	$HNO_3 + hv = NO_2 + OH$
56	$NO + hv = N + O$
57	$NO_2 + hv = NO + O$
58	$CH_4 + OH = CH_3 + H_2O$
59	$CH_4 + O(^1D) = CH_3 + OH$
60	$CH_4 + O(^1D) = H_2CO + H_2$
61	$1CH_2 + CH_4 = 2\ CH_3$
62	$1CH_2 + O_2 = HCO + OH$
63	$1CH_2 + M = {}^3CH_2 + M$
64	$^3CH_2 + H_2 = CH_3 + H$
65	$^3CH_2 + CH_4 = 2CH_3$
66	$^3CH_2 + O_2 = HCO + OH$
67	$CH_3 + O_2 + M = H_2CO + OH$
68	$CH_3 + OH = H_2CO + H_2$
69	$CH_3 + O = H_2CO + H$
70	$CH_3 + O_3 = H_2CO + HO_2$
71	$CH_3 + CH_3 + M = C_2H_6 + M$
72	$CH_3 + hv = 1CH_2 + H$
73	$CH_3 + H + M = CH_4 + M$
74	$CH_3 + HCO = CH_4 + CO$
75	$CH_3 + HNO = CH_4 + NO$
76	$CH_3 + H_2CO = CH_4 + HCO$
77	$H + NO + M = HNO + M$
78	$N + N + M = N_2 + M$
79	$N + O_2 = NO + O$
80	$N + O_3 = NO + O_2$
81	$N + OH = NO + H$
82	$N + NO = N_2 + O$
83	$NO + O_3 = NO_2 + O_2$
84	$NO + O + M = NO_2 + M$

85	$NO + HO_2 = NO_2 + OH$
86	$NO + OH + M = HNO_2 + M$
87	$NO_2 + O = NO + O_2$
88	$NO_2 + OH + M = HNO_3 + M$
89	$NO_2 + H = NO + OH$
90	$HNO_3 + OH = H_2O + NO_2 + O$
91	$HCO + NO = HNO + CO$
92	$HNO + hv = NO + H$
93	$H + HNO = H_2 + NO$
94	$O + HNO = OH + NO$
95	$OH + HNO = H_2O + NO$
96	$HNO_2 + OH = H_2O + NO_2$
97	$CH_4 + O = CH_3 + OH$
98	$1CH_2 + H_2 = CH_3 + H$
99	$1CH_2 + CO_2 = H_2CO + CO$
100	$^3CH_2 + O = HCO + H$
101	$^3CH_2 + CO_2 = H_2CO + CO$
102	$C_2H_6 + OH = C_2H_5 + H_2O$
103	$C_2H_6 + O = C_2H_5 + OH$
104	$C_2H_6 + O(^1D) = C_2H_5 + OH$
105	$C_2H_5 + H = CH_3 + CH_3$
106	$C_2H_5 + O = CH_3 + HCO + H$
107	$C_2H_5 + OH = CH_3 + HCO + H_2$
108	$C_2H_5 + HCO = C_2H_6 + CO$
109	$C_2H_5 + HNO = C_2H_6 + NO$
110	$C_2H_5 + O_2 + M = CH_3 + HCO + OH$
111	$SO + hv = S + O$
112	$SO_2 + hv = SO + O$
113	$H_2S + hv = HS + H$
114	$SO + O_2 = O + SO_2$
115	$SO + HO_2 = SO_2 + OH$
116	$SO + O + M = SO_2 + M$
117	$SO + OH = SO_2 + H$
118	$SO_2 + OH + M = HSO_3 + M$
119	$SO_2 + O + M = M + SO_3$
120	$SO_3 + H_2O = H_2SO_4$
121	$HSO_3 + O_2 = HO_2 + SO_3$
122	$HSO_3 + OH = H_2O + SO_3$
123	$HSO_3 + H = H_2 + SO_3$
124	$HSO_3 + O = OH + SO_3$
125	$H_2S + OH = H_2O + HS$
126	$H_2S + H = H_2 + HS$
127	$H_2S + O = OH + HS$
128	$HS + O = H + SO$
129	$HS + O_2 = OH + SO$

130	$HS + HO_2 = H_2S + O_2$
131	$HS + HS = H_2S + S$
132	$HS + HCO = H_2S + CO$
133	$HS + H = H_2 + S$
134	$HS + S = H + S_2$
135	$S + O_2 = SO + O$
136	$S + OH = SO + H$
137	$S + HCO = HS + CO$
138	$S + HO_2 = HS + O_2$
139	$S + HO_2 = SO + OH$
140	$S + S = S_2$
141	$S_2 + OH = HSO + S$
142	$S_2 + O = S + SO$
143	$SH + H_2CO = H_2S + HCO$
144	$SO_2 + hv = SO_2^1$
145	$SO_2 + hv = SO_2^3$
146	$S_2 + hv = S + S$
147	$S_2 + hv = S_2^*$
148	$H_2SO_4 + hv = SO_2 + {}_2\,OH$
149	$SO_3 + hv = SO_2 + O$
150	$SO_2(^1B) + M = SO_2(^3B) + M$
151	$SO_2(^1B) + M = SO_2 + M$
152	$SO_2(^1B) = SO_2(^3B) + hv$
153	$SO_2(^1B) = SO_2 + hv$
154	$SO_2(^1B) + O_2 = SO_3 + O$
155	$SO_2(^1B) + SO_2 = SO_3 + SO$
156	$SO_2(^3B) + M = SO_2 + M$
157	$SO_2(^3B) = SO_2 + hv$
158	$SO_2(^3B) + SO_2 = SO_3 + SO$
159	$SO + NO_2 = SO_2 + NO$
160	$SO + O_3 = SO_2 + O_2$
161	$CSO_2 + HO_2 = SO_3 + OH$
162	$HS + O_3 = HSO + O_2$
163	$HS + NO_2 = HSO + NO$
164	$S + O_3 = SO + O_2$
165	$SO + SO = SO_2 + S$
166	$SO_3 + SO = SO_2 + SO_2$
167	$S + CO_2 = SO + CO$
168	$SO + HO_2 = HSO + O_2$
169	$SO + HCO = HSO + CO$
170	$H + SO + M = HSO + M$
171	$HSO + hv = HS + O$
172	$HSO + NO = HNO + SO$
173	$HSO + OH = H_2O + SO$
174	$HSO + H = HS + OH$

175	$HSO + H = H_2 + SO$
176	$HSO + HS = H_2S + SO$
177	$HSO + O = OH + SO$
178	$HSO + S = HS + SO$
179	$S + S_2 + M = S_3 + M$
180	$S_2 + S_2 + M = S_4 + M$
181	$S + S_3 + M = S_4 + M$
182	$S_4 + S_4 + M = S_8(AER) + M$
183	$S_4 + hv = S_2 + S_2$
184	$S_3 + hv = S_2 + S$
185	$NH_3 + hv = NH_2 + H$
186	$NH_3 + OH = NH_2 + H_2O$
187	$NH_3 + O(^1D) = NH_2 + OH$
188	$NH_2 + H + M = NH_3 + M$
189	$NH_2 + NO = N_2 + H_2O$
190	$NH_2 + NH_2 + M = N_2H_4 + M$
191	$NH_2 + O = NH + OH$
192	$NH_2 + O = HNO + H$
193	$NH + NO = N_2 + O + H$
194	$NH + O = N + OH$
195	$N_2H_4 + hv = N_2H_3 + H$
196	$N_2H_4 + H = N_2H_3 + H_2$
197	$N_2H_3 + H = 2NH_2$
198	$N_2H_3 + N_2H_3 = N_2H_4 + N_2 + H_2$
199	$NH + H + M = NH_2 + M$
200	$NH + hv = N + H$
201	$NH_2 + hv = NH + H$
202	$NH_2 + hv = NH_2^*$
203	$NH_2^* = NH_2 + hv$
204	$NH_2^* + M = NH_2 + M$
205	$NH_2^* + H_2 = NH_3 + H$
206	$NH_2 + HCO = NH_3 + CO$
207	$NH + HCO = NH_2 + CO$
208	$^1CH_2 + O_2 = H_2CO + O$
209	$^3CH_2 + O_2 = H_2CO + O$
210	$C_2H_2 + hv = C_2H + H$
211	$C_2H_2 + hv = C_2 + H_2$
212	$C_2H_4 + hv = C_2H_2 + H_2$
213	$^3CH_2 + CH_3 = C_2H_4 + H$
214	$C_2H_5 + CH_3 + M = C_3H_8 + M$
215	$C_3H_8 + OH = C_3H_7 + H_2O$
216	$C_3H_8 + O = C_3H_7 + OH$
217	$C_3H_8 + O(^1D) = C_3H_7 + OH$
218	$C_3H_7 + H = CH_3 + C_2H_5$
219	$_3CH_2 + _3CH_2 = C_2H_2 + H + H$

220	$C_2H_2 + OH = CO + CH_3$
221	$C_2H_2 + H + M = C_2H_3 + M$
222	$C_2H_3 + H = C_2H_2 + H_2$
223	$C_2H_3 + H_2 = C_2H_4 + H$
224	$C_2H_3 + CH_4 = C_2H_4 + CH_3$
225	$C_2H_3 + C_2H6 = C_2H_4 + C_2H_5$
226	$C_2H_4 + OH = H_2CO + CH_3$
227	$C_2H_4 + O = HCO + CH_3$
228	$C_2H_4 + H + M = C_2H_5 + M$
229	$C_2H + O_2 = CO + HCO$
230	$C_2H + H_2 = C_2H_2 + H$
231	$C_2H + CH_4 = C_2H_2 + CH_3$
232	$C_2H + C_2H_6 = C_2H_2 + C_2H_5$
233	$C_2H + H + M = C_2H_2 + M$
234	$C_3H_8 + hv = C_3H_6 + H_2$
235	$C_3H_8 + hv = C_2H_6 + 1CH_2$
236	$C_3H_8 + hv = C_2H_4 + CH_4$
237	$C_3H_8 + hv = C_2H5 + CH_3$
238	$CC_2H_6 + hv = C_2H_2 + H_2 + H_2$
239	$C_2H_6 + hv = C_2H_4 + H + H$
240	$C_2H_6 + hv = C_2H_4 + H_2$
241	$C_2H_6 + hv = {}^2CH_3$
242	$C_2H_4 + hv = C_2H_2 + H + H$
243	$C_3H_6 + hv = C_2H_2 + CH_3 + H$
244	$CH_4 + hv = {}^3CH_2 + {}_2H$
245	$CH_4 + hv = CH_3 + H$
246	$CH + hv = C + H$
247	$CH_2CO + hv = {}^3CH_2 + CO$
248	$CH_3CHO + hv = CH_3 + HCO$
249	$CH_3CHO + hv = CH_4 + CO$
250	$C_2H_5CHO + hv = C_2H_5 + HCO$
251	$C_3H_3 + hv = C_3H_2 + H$
252	$CH_3C_2H + hv = C_3H_3 + H$
253	$CCH_3C_2H + hv = C_3H_2 + H_2$
254	$CH_3C_2H + hv = CH_3 + C_2H$
255	$CH_2CCH_2 + hv = C_3H_3 + H$
256	$CCH_2CCH_2 + hv = C_3H_2 + H_2$
257	$CH_2CCH_2 + hv = C_2H_2 + {}^3CH_2$
258	$C_3H_6 + hv = CH_2CCH_2 + H_2$
259	$C_3H_6 + hv = C_2H_4 + {}^3CH_2$
260	$C_3H_6 + hv = C_2H + CH_4 + H$
261	$C + OH = CO + H$
262	$C + H_2 + M = {}^3CH_2 + M$
263	$C + O_2 = CO + O$
264	$CH + H = C + H_2$

265	$CH + O = CO + H$
266	$CH + H_2 = {}^3CH_2 + H$
267	$CH + H_2 + M = CH_3 + M$
268	$CH + O_2 = CO + OH$
269	$CH + CO_2 = HCO + CO$
270	$CH + CH_4 = C_2H_4 + H$
271	$CH + C_2H_2 = C_3H_2 + H$
272	$CH + C_2H_4 = CH_3C_2H + H$
273	$CH + C_2H_4 = CH_2CCH_2 + H$
274	${}^3CH_2 + O = CH + OH$
275	${}^3CH_2 + O = CO + H + H$
276	${}^3CH_2 + H + M = CH_3 + M$
277	${}^3CH_2 + H = CH + H_2$
278	${}^3CH_2 + CO + M = CH_2CO + M$
279	${}^3CH_2 + {}^3CH_2 = C_2H_2 + H_2$
280	${}^3CH_2 + C_2H_2 + M = CH_3C_2H + M$
281	${}^3CH_2 + C_2H_3 = CH_3 + C_2H_2$
282	${}^3CH_2 + C_2H_5 = CH_3 + C_2H_4$
283	$CH_2CO + H = CH_3 + CO$
284	$CH_2CO + O = H_2CO + CO$
285	$CH_2CCH_2 + H + M = CH_3 + C_2H_2 + M$
286	$CH_2CCH_2 + H + M = C_3H_5 + M$
287	$CCH_3 + O_2 + M = CH_3O_2 + M$
288	$CH_3 + CO + M = CH_3CO + M$
289	$CH_3 + H_2CO = CH_4 + HCO$
290	$CH_3 + OH = CO + H_2 + H_2$
291	$CH_3 + C_2H_3 = C_3H_5 + H$
292	$CH_3O_2 + H = CH_4 + O_2$
293	$CH_3O_2 + H = H_2O + H_2CO$
294	$CH_3O_2 + O = H_2CO + HO_2$
295	$CH_3CO + H = CH_4 + CO$
296	$CH_3CO + O = H_2CO + HCO$
297	$CH_3CO + CH_3 = C_2H_6 + CO$
298	$CH_3CO + CH_3 = CH_4 + CH_2CO$
299	$CH_3CHO + H = CH_3CO + H_2$
300	$CH_3CHO + O = CH_3CO + OH$
301	$CH_3CHO + OH = CH_3CO + H_2O$
302	$CH_3CHO + CH_3 = CH_3CO + CH_4$
303	$CH_3C_2H + H + M = CH_3 + C_2H_2 + M$
304	$CH_3C_2H + H + M = C_3H_5 + M$
305	$C_2 + O = C + CO$
306	$C_2 + O_2 = CO + CO$
307	$C_2 + H_2 = C_2H + H$
308	$C_2 + CH_4 = C_2H + CH_3$
309	$C_2H + O = CO + CH$

310	$C_2H + C_3H_8 = C_2H_2 + C_3H_7$
311	$C_2H_2 + O = {}^3CH_2 + CO$
312	$C_2H_2 + OH = C_2H_2OH$
313	$C_2H_2 + OH + M = CH_2CO + H + M$
314	$C_2H_2OH + H = H_2O + C_2H_2$
315	$C_2H_2OH + H = H_2 + CH_2CO$
316	$C_2H_2OH + O = OH + CH_2CO$
317	$C_2H_2OH + OH = H_2O + CH_2CO$
318	$C_2H_3 + O = CH_2CO + H$
319	$C_2H_3 + OH = C_2H_2 + H_2O$
320	$C_2H_3 + CH_3 = C_2H_2 + CH_4$
321	$C_2H_3 + CH_3 + M = C_3H_6 + M$
322	$C_2H_3 + C_2H_3 = C_2H_4 + C_2H_2$
323	$C_2H_3 + C_2H_5 = C_2H_4 + C_2H_4$
324	$C_2H_3 + C_2H_5 = CH_3 + C_3H_5$
325	$C_2H_4 + OH + M = C_2H_4OH + M$
326	$C_2H_4OH + H = H_2O + C_2H_4$
327	$C_2H_4OH + H = H_2 + CH_3CHO$
328	$C_2H_4OH + O = OH + CH_3CHO$
329	$C_2H_4OH + OH = H_2O + CH_3CHO$
330	$C_2H_5 + OH = CH_3CHO + H_2$
331	$C_2H_5 + O = CH_3CHO + H$
332	$C_2H_5 + CH_3 = C_2H_4 + CH_4$
333	$C_2H_5 + C_2H_3 = C_2H_6 + C_2H_2$
334	$C_2H_5 + C_2H_5 = C_2H_6 + C_2H_4$
335	$C_2H_5 + H + M = C_2H_6 + M$
336	$C_2H_5 + H = C_2H_4 + H_2$
337	$C_3H_2 + H + M = C_3H_3 + M$
338	$C_3H_3 + H + M = CH_3C_2H + M$
339	$C_3H_3 + H + M = CH_2CCH_2 + M$
340	$C_3H_5 + H = CH_3C_2H + H_2$
341	$C_3H_5 + H + M = C_3H_6 + M$
342	$C_3H_5 + H = CH_4 + C_2H_2$
343	$C_3H_5 + CH_3 = CH_3C_2H + CH_4$
344	$C_3H_5 + CH_3 = CH_2CCH_2 + CH_4$
345	$C_3H_6 + OH = CH_3CHO + CH_3$
346	$C_3H_6 + O = CH_3 + CH_3 + CO$
347	$C_3H_6 + H + M = C_3H_7 + M$
348	$C_3H_7 + CH_3 = C_3H_6 + CH_4$
349	$C_3H_7 + OH = C_2H_5CHO + H_2$
350	$C_3H_7 + O = C_2H_5CHO + H$
351	$H + CH_2CCH_2 = CH_3C_2H + H$
352	$O + H_2CO = OH + HCO$
353	$^3CH_2 + C_2H_2 + M = CH_2CCH_2 + M$
354	$C_2H + C_2H_2 = HCAER + H$

355	$^1CH_2 + H_2 = {}^3CH_2 + H_2$
356	$C_3H_5 + H = CH_2CCH_2 + H_2$
357	$HCO + H_2CO = CH_3O + CO$
358	$CH_3O + CO = CH_3 + CO_2$
359	$C_2H + CH_2CCH_2 = HCAER + H$

ACADEMIC VITA of Megan Leigh Smith

Megan Leigh Smith
224 S. Burrowes St. Apt #203
State College, PA 16801
meg.smith.psu@gmail.com

Education:

Bachelor of Science Degree in Meteorology, Penn State University, Spring 2010
Minor in Astrobiology
Honors in Meteorology
Thesis Title: Investigation of a Possible Solution to the Faint Young Sun Paradox: Elemental Sulfur Aerosols
Thesis Supervisor: Dr. James F. Kasting

Related Experience:

Internship with the National Geospatial-Intelligence Agency
Supervisor: Dr. Ronald Resmini
Summer 2008

Research Assistant with the Penn State Department of Geosciences
Supervisor: Dr. James F. Kasting
Summer 2009

Awards:

Deans List
Phi Kappa Phi Honors Society
Sylvia Stein Memorial Space Grant Scholarship, 2009-2010

Presentations/Activities:

Attendee of the Sagan Exoplanet Summer Workshop, 2009